which should be cited to refer to this work.

Characterization of large area avalanche photodiodes in X-ray and VUV-light detection

L.M.P. Fernandes,[a*] F.D. Amaro,[a] A. Antognini,[b] J.M.R. Cardoso,[a] C.A.N. Conde,[a] O. Huot,[c] P.E. Knowles,[c] F. Kottmann,[d] J.A.M. Lopes,[a] L. Ludhova,[cd] C.M.B. Monteiro,[a] F. Mulhauser,[c] R. Pohl,[bd] J.M.F. dos Santos,[a] L.A. Schaller,[c] D. Taqqu[d] and J.F.C.A. Veloso[e]

[a] *Physics Department, University of Coimbra, P-3004-516 Coimbra, Portugal*
[b] *Max-Planck Institut für Quantenoptik, D-85748 Garching, Germany*
[c] *Physics Department, University of Fribourg, CH-1700 Fribourg, Switzerland*
[d] *Paul Scherrer Institute, CH-5232 Villigen PSI, Switzerland*
[e] *Physics Department, University of Aveiro, P-3810-193 Aveiro, Portugal*
E-mail: pancho@gian.fis.uc.pt

ABSTRACT: The present manuscript reviews our R&D studies on the application of large area avalanche photodiodes (LAAPDs) to the detection of X-rays and vacuum ultraviolet (VUV) light. The operational characteristics of LAAPDs manufactured by Advanced Photonix Inc. were investigated for X-ray detection at room temperature. The optimum energy resolution obtained in four LAAPDs investigated was found to be in the range 10-18% for 5.9 keV X-rays. The observed variations are associated with dark current differences between the several prototypes. LAAPDs have demonstrated high counting rate capability (up to about 10^5/s) and applicability in diverse areas, mainly low-energy X-ray detection, where LAAPDs selected for low dark current may achieve better performance than proportional counters. LAAPDs were also investigated as VUV photosensors, presenting advantages compared to photomultiplier tubes. X-rays are often used as a reference in light measurements; this may be compromised by the non-linearity between gains measured for X-rays and VUV-light. The gain was found to be lower for X-rays than for VUV light, especially at higher bias voltages. For 5.9 keV X-rays, gain variations of 10% and 6% were measured relative to VUV light produced in argon (~128 nm) and xenon (~172 nm) for gains of about 200. The effect of temperature on the LAAPD performance was investigated for X-ray and VUV-light detection. Gain variations of more than -4% per ºC were measured for 5.9 keV X-rays for gains above 200, while for VUV light variations are larger than -5% per ºC. The energy resolution was found to improve with decreasing temperature, what is mainly attributed to dark current. The excess noise factor, another contribution to the energy resolution, was experimentally determined and found to be independent of temperature, increasing linearly with gain, from 1.8 to 2.3 for a 50-300 gain range. The LAAPD response under intense magnetic fields up to 5 Tesla was investigated. While for X-ray detection the APD response practically does not vary with the magnetic field, for 172 nm VUV light a significant amplitude reduction of more than 20% was observed.

KEYWORDS: X-ray detectors; Photon detectors for UV, visible and IR photons (solid-state); Spectrometers.

* Corresponding author.

Contents

1. Introduction

Avalanche PhotoDiodes (APDs) are monolithic devices made of silicon p-n junctions. They have been used as radiation detectors in an increasing number of applications due to their compact structure, simple operation, low power consumption and sensitivity to different radiation types. APDs are able to detect light in the whole visible spectrum, from the infrared to the Vacuum UltraViolet (VUV) regions, and X-rays with energy up to about 25 keV.

In the last years, significant advances in the development of Large-Area Avalanche PhotoDiodes (LAAPDs) triggered the characterization of different commercially available APDs [1]-[4]. They have been used mainly as optical photosensors coupled to scintillators for X-ray, γ-ray and particle detection in applications such as the electromagnetic calorimeter of the Compact Muon Solenoid (CMS) experiment at the Large Hadron Collider (LHC) [2],[3], Positron Emission Tomography (PET) instrumentation [5],[6] and nuclear physics [1],[4].

More recently, windowless LAAPDs with spectral response extended down to the VUV region (down to 120 nm) have been developed by API (Advanced Photonix Inc., 1240 Avenida Acaso, Camarillo, CA 93012, U.S.A.). As a result of their enhanced quantum efficiency, these LAAPDs can replace PhotoMultiplier Tubes (PMTs) or CsI-based photosensors in applications where the high gain is not the most important parameter, such as the detection of the primary and secondary scintillation of rare gases in gas proportional scintillation counters [7],[8].

The feasibility of using LAAPDs as X-ray detectors was previously demonstrated [9],[10]. Although their use for X-ray detection in the energy range 0.5-20 keV was suggested [11]-[13], low-energy X-ray detection techniques with APDs were mainly developed to measure the number of charge carriers in light measurements, using X-rays as a reference [11],[13]-[15].

The objective of our studies with LAAPDs was to investigate their response as direct X-ray detectors, for X-ray spectrometry applications, and as VUV photosensors in Gas Proportional Scintillation Counters (GPSCs). Studies with X-rays include the operational characteristics at room temperature [16], behaviour under intense magnetic fields (up to 5 Tesla) [17],[18], the effect of temperature on the LAAPD gain and performance [19]-[21] and the application to X-ray spectrometry.

Concerning the use of LAAPDs as VUV photosensors in GPSCs [7],[8],[22], their response to VUV-light pulses from argon (~128 nm) and xenon (~172 nm) scintillation was investigated. Their operational characteristics for VUV-light detection were studied, including the gain non-linearity between X-rays and VUV light [23], the behaviour under intense magnetic fields [17], the temperature dependence of the LAAPD response, including gain, minimum detection limit and statistical fluctuations [24].

2. The avalanche photodiode

For a long time, only PhotoMultiplier Tubes (PMTs) and conventional photodiodes provided quantitative detection over the whole visible light spectrum. The avalanche photodiode combines the benefits of both photosensors as it is a silicon photodiode with internal gain. The gain is however significantly lower than that obtained with a PMT, reaching less than 10^3. The gain is obtained by applying a high reverse bias voltage to the photodiode which creates an intense electric field inside its volume.

Non-uniformity has been a major drawback in the manufacture of LAAPDs, limiting their applications. However, LAAPDs from API have been developed with improved spatial uniformity, delivering higher gains at lower bias voltages [14]. Comparing to others, LAAPDs from API have higher quantum efficiency and lower noise levels [25]. The basis of the API technology is the development of silicon crystals with n-type doping obtained by neutron transmutation, with more uniform resistivity, which provides larger avalanche regions with more moderate electric fields and therefore lower dark current. According to API, only crystals with resistivity variations lower than 5% are used in the manufacture of LAAPDs.

When a reverse bias voltage is applied to the APD, the maximum electric field is reached around the p-n junction and, at higher voltages, the field could be so strong to cause breakdown at the junction edges. To prevent this problem, LAAPDs from API have bevelled edge geometry with reduced electric field strength in the junction edges.

2.1 Structure and response

Figure 1 shows the structure of a bevelled edge LAAPD and, showing the electric field profile inside its volume. When a high voltage is applied to the LAAPD, only a small region of the p-layer near the APD surface, the drift region (i), remains undepleted. This region shows a residual electric field of about 50 V/cm [26] due to the high acceptor concentration. In the depleted p-region, the electric field increases with depth until reaching a maximum, about 1.8×10^5 V/cm [26], near the p-n junction, and then decreases in the depleted n-region. In the front portion of the depleted p-region (ii), the electric field is not enough to provide electron

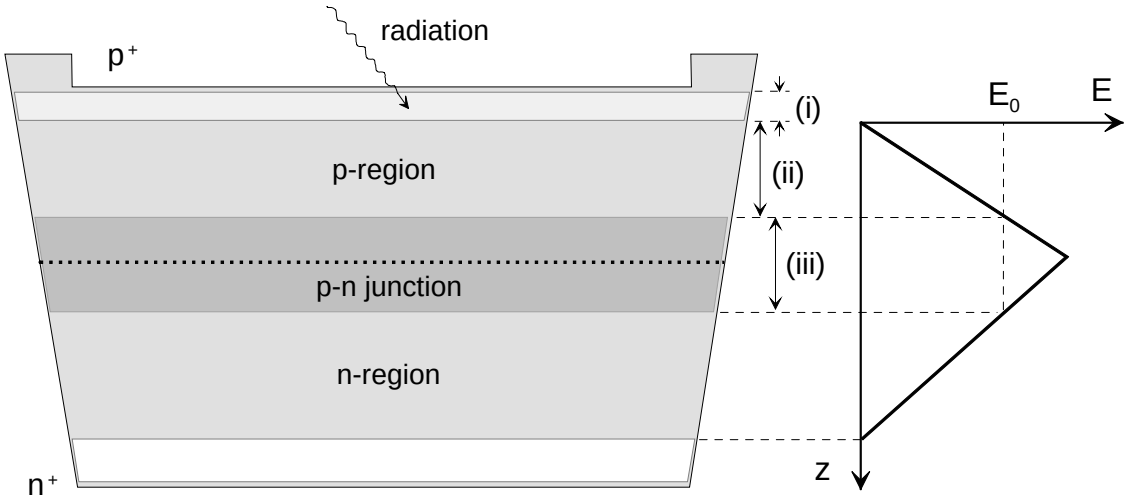

Figure 1. Section of a bevelled edge avalanche photodiode and electric field profile across its volume. The silicon active region of the APD is divided in three different parts: the drift region (i), the front portion of the depleted p-region (ii) and the multiplication region (iii). E_0 is the minimum electric field where electron multiplication takes place.

multiplication. The multiplication region (iii) starts when the electric field exceeds the threshold for electron multiplication (E_0).

Light photons, X-rays or charged particles absorbed in the p-region of the APD are converted into electron-hole pairs. The resulting primary electrons are driven to the p-n junction by the electric field. Around the junction, they obtain a sufficient amount of energy to produce new electron-hole pairs by impact ionization, originating an avalanche process in the multiplication region. Charge gains of a few hundred are typical. The gain increases supra-exponentially with the applied voltage, resulting in a significant improvement of the signal-to-noise ratio [9],[14],[27].

The silicon active thickness extends from the APD surface to the multiplication region edge in the n-region side. The X-ray response of the APD can be understood by considering the locations where X-rays are absorbed. The active region can be divided in three different regions of interest: the drift region (i), the front portion of the depleted p-region (ii) and the multiplication region (iii), as shown in figure 1. Due to the weak electric field in region (i), X-rays absorbed there produce electrons that will be slowly transported to the edge of the depletion region, originating delayed pulses. In addition, traps in this region may hold electrons for long periods of time (tens to thousands of ns [27]), causing a reduction in the amplitude of the current pulse getting to the high-field region and possibly a reduction in the output pulse amplitude, depending on the signal integration time. X-rays absorbed in region (ii) generate fully amplified pulses with faster time response compared to X-rays absorbed in the drift region. The primary electrons drift rapidly to the high electric field region, undergoing an average amplification equal to the APD gain. X-rays absorbed in the multiplication region produce electrons that will be partially amplified, creating pulses with lower amplitude and faster time response. As X-rays with the same energy can be absorbed in any of the regions (i), (ii) or (iii), the amplitude distribution of the APD output signals deviates from a Gaussian curve due to a low-energy tail associated with pulses of lower amplitude generated in the regions (i) and (iii).

When a voltage is applied to an APD in order to polarize its p-n junction, a current with low intensity, typically a fraction of μA, is observed. This dark current is originated in the detector volume and surface. The volumetric dark current results from the continuous generation of charges (minority carriers) in both sides of the junction, which are conducted through it, and from the thermal generation of electron-hole pairs in the depletion region, which decreases by cooling. The superficial dark current is generated at the p-n junction edges due to high voltage gradients. Since dark current is a noise source and increases considerably with temperature, the electronic noise level can be reduced by cooling the APD.

The APD response depends on the photon penetration depth. For VUV-light, as the penetration depth is only 5-6 nm at λ ~170 nm [28], the photon absorption takes place in the first layers of silicon. For visible light, the penetration depth is about 1 μm and photons are absorbed deeper compared to VUV photons but still before the multiplication region. In both cases, the LAAPD response does not vary significantly from event to event. In contrast, X-rays can interact in different regions of the APD, creating pulses with different amplitudes and time responses.

In X-ray detection, the majority of X-rays absorbed create fast electrons for which the total energy is approximately equal to the incident photon energy. These electrons are stopped in successive collisions and create on average one electron-hole pair per each 3.62 eV of energy deposited in silicon [29]. Each X-ray absorbed in the APD can thus be considered as a local deposition of E/ε electron-hole pairs, E being the energy of the incident X-ray and ε the average energy required to create an electron-hole pair in silicon (3.62 eV).

The APD detection efficiency for X-rays depends on their penetration depth in silicon, which is about 30 μm for 6 keV X-rays and increases rapidly with the energy, reaching about 70, 130 and 450 μm for energies of 8, 10 and 15 keV, respectively [30]. As the active region thickness is about 12 μm for LAAPDs from API, the APD detection efficiency, defined as the ratio between the number of fully amplified pulses at the APD output and the number of photons incident in the APD surface, decreases rapidly for energies above 6 keV, being about 45, 25, 8 and 4% for 8, 10, 15 and 20 keV energies, respectively [11],[27].

2.2 Energy resolution

The energy resolution associated with radiation detection in avalanche photodiodes is determined by several factors:

- statistical fluctuations associated with the number of electron-hole pairs created in silicon and the avalanche process (ΔE_S);
- gain non-uniformity in the APD detection volume (ΔE_U);
- detector noise (resulting from dark current) and electronic system noise (ΔE_N).

The total broadening (ΔE) in the energy distributions for APD signals is the quadratic addition of the three contributions:

$$\Delta E^2 = \Delta E_S{}^2 + \Delta E_U{}^2 + \Delta E_N{}^2. \quad (2.1)$$

The output signal variance associated to the statistical contribution is given, in number of primary electrons, by [29],[31]:

$$\sigma_S{}^2 = \sigma_n{}^2 + N\,(F-1), \quad (2.2)$$

N being the number of primary electrons, $\sigma_n{}^2$ its variance and F the excess noise factor, which is related to the variance of the electron avalanche gain, $\sigma_A{}^2$, according to:

$$F = 1 + \sigma_A{}^2 / G^2. \quad (2.3)$$

As the discrete nature of the multiplication process results in electron avalanche fluctuations, F is higher than 1 and varies with the gain, G.

There are significant differences on the APD response in light and X-ray detection. In particular, the non-uniformity contribution is negligible in light detection if the whole area is irradiated as the final pulse results from the average response to the full amount of photons interacting in the silicon. In X-ray detection, each pulse is locally created and the final distribution is affected by the position gain variation.

For light detection, the variance of the number of primary electrons is described by Poisson statistics, with $\sigma_n^2 = N$. The statistical contribution then is:

$$\sigma_S^2 = N F. \tag{2.4}$$

The intrinsic resolution (total energy resolution without the noise contribution) for light detection is basically determined by the statistical contribution:

$$R_{\text{int}} = 2.36 \frac{\sigma_S}{N} = 2.36 \sqrt{\frac{F}{N}}. \tag{2.5}$$

For X-ray detection, the peak broadening process is more complex. The statistical fluctuations associated with primary electrons are attenuated by the Fano factor f. In silicon, f is about 0.12 for 5.9 keV X-rays [32]. The variance of the number of primary electrons is now $\sigma_n^2 = N f$ and the statistical contribution to the energy resolution is:

$$\sigma_S^2 = N (F + f - 1). \tag{2.6}$$

The energy resolution for X-rays can be seriously degraded due to the gain non-uniformity. If σ_U / G is the relative standard deviation associated with the gain non-uniformity, the intrinsic resolution for X-rays can be described by:

$$R_{\text{int}} = 2.36 \sqrt{\frac{F + f - 1}{N} + \left(\frac{\sigma_U}{G} \right)^2}. \tag{2.7}$$

The noise contribution to the energy resolution has two different sources: the detector dark current and the electronic system. Dark current has two different components. One (I_{DS}) corresponds to the superficial current and to a small fraction of the volumetric current resulting from the thermal generation of electron-hole pairs in the n-region. This component does not depend on the APD gain. The other component (I_{DV}) corresponds to the volumetric current resulting from the generation of electron-hole pairs in the p-region and is amplified by the gain.

The total current at the APD output is:

$$I = I_{DS} + G I_{DV} + G I_0 \tag{2.8}$$

where G is the APD gain and I_0 the non-amplified signal current, corresponding to the electron-hole pairs produced by the radiation absorbed.

The electronic system noise mainly originates in the FET (field effect transistor) at the preamplifier input. Fluctuations in the FET channel current are similar to thermal noise and can be represented by a noise equivalent resistance (R_{eq}) in series with the preamplifier input [33]. A

detailed noise analysis in avalanche photodiodes is presented in the literature [12],[34]. If a charge preamplifier is connected to a linear amplifier with equal differentiation and integration constants τ, the electronic noise contribution to the peak broadening (in units of energy) is:

$$\Delta E_N{}^2 = \left(2.36\frac{e\varepsilon}{qG}\right)^2\left[\frac{k_B T R_{eq}}{2\tau}C_T{}^2 + \frac{\tau q}{4}(I_{DS} + I_{DV} G^2 F)\right] \tag{2.9}$$

q being the electron charge, $e \cong 2.718$ the number of Nepper, k_B the Boltzmann constant (1.38×10^{-23} J/K), T the temperature (in Kelvin) and C_T the total capacitance at the preamplifier input (including detector and FET input capacitances).

The total energy resolution is given by the equation:

$$R^2 = R_{\text{int}}{}^2 + \left(2.36\frac{e\varepsilon}{qEG}\right)^2\left[\frac{k_B T R_{eq}}{2\tau}C_T{}^2 + \frac{\tau q}{4}(I_{DS} + I_{DV} G^2 F)\right] \tag{2.10}$$

where R_{int} is the intrinsic resolution, given by eq. (2.5) and eq. (2.7) for light and X-ray detection, respectively, and E is the energy deposited in silicon by the incident radiation.

The relationship between F and G can be derived from the McIntyre model assuming that photoelectrons are injected next to the p-zone surface [35]:

$$F \cong G\,k_{ef} + \left(2 - \frac{1}{G}\right)\left(1 - k_{ef}\right) \tag{2.11}$$

k_{ef} being the effective ratio between the ionization coefficients for holes and electrons. For low gains, $k_{ef} << 1$ and then $F \cong 2 - 1/G$. For useful gains (above 30), the variation of k_{ef} with the bias voltage is very soft and k_{ef} can be considered a constant. As a result, F has an approximately linear dependence of G.

The energy resolution can be estimated from eqs. (2.10) and (2.11). Typical values for LAAPDs from API, with 16 mm diameter, are dark current components $I_{DS} = 100$ nA and $I_{DV} = 0.3$ nA at room temperature and $k_{ef} \approx 0.0015$ [36]. The LAAPD capacitance is about 130 pF [26]. Using a charge sensitive preamplifier with a JFET mutual conductance of 20 mS and an input capacitance of 1 pF, then $R_{eq} \cong 33\,\Omega$ [33] and $C_T \cong 130$ pF. Under the previous conditions and assuming shaping time constants of 200 ns and a gain non-uniformity of 2% (standard deviation), the energy resolution estimated for 6 keV X-rays reaches a minimum value of about 10% at a gain of 100. The energy resolution increases with decreasing energy, as results from eq. (2.10). An optimum value of 21% is estimatedfor for 2 keV X-rays at a gain of 125 . As the gain non-uniformity and dark current may vary considerably from prototype to prototype, we expect significant differences on both the intrinsic resolution and noise contribution.

3. X-ray detection

The LAAPD performance characteristics were determined at room temperature for X-ray detection, including gain and energy resolution measurements and the study of the spatial uniformity, the counting rate capability and space charge effects. The variation of the LAAPD gain and dark current with temperature was determined and its influence on the LAAPD performance was investigated. The behaviour of LAAPDs under intense magnetic fields (up to 5 T) was investigated and finally their application to X-ray spectrometry was evaluated at room and lower temperatures.

LAAPD No.	Diameter (mm)	Voltage (V)	Gain	Dark Current (nA)
1	16	1840	317	201
2	16	1851	312	336
3	16	1849	303	499
4	16	1873	314	222

Table 1. LAAPD specifications just before breakdown, according to the manufacturer.

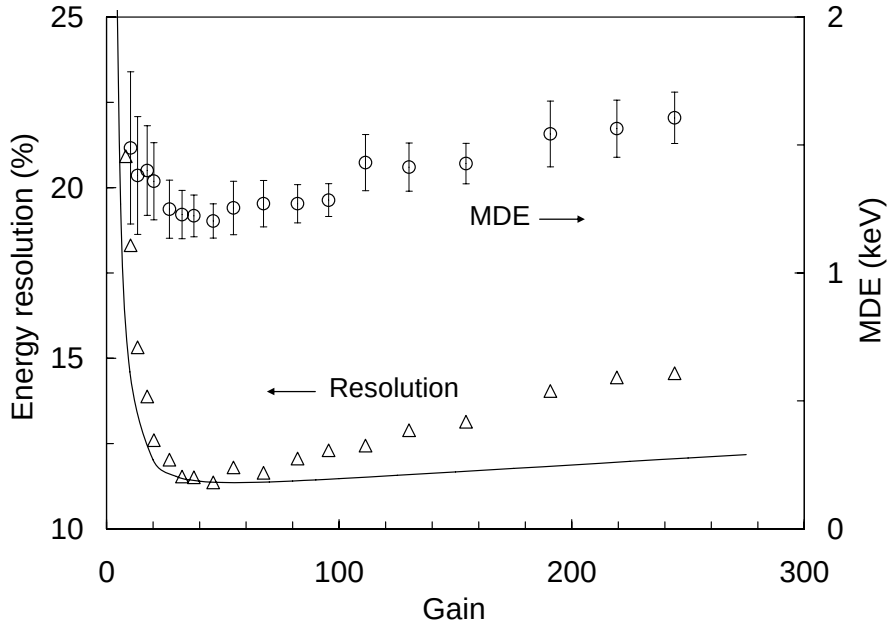

Figure 2. Energy resolution for 5.9 keV X-rays and minimum detectable energy (MDE) as a function of the gain for LAAPD 4 (table 1). The energy resolution experimental errors fall within the symbol size. The curve is an estimate of the energy resolution, eq. (2.10).

3.1 Response characteristics at room temperature

Several windowless UV-enhanced LAAPDs from API were investigated. The characteristics of each LAAPD were evaluated with 5.9 keV X-rays from a ^{55}Fe source (Mn K_α-line). The Mn K_β-line (6.4 keV X-rays) was efficiently reduced by absorption in a chromium foil (15 μm thick), which attenuates the K_α-line by 50% and the K_β-line by 99%. Table 1 shows the main specifications for each LAAPD according to the manufacturer supplied data sheets.

The X-ray signals obtained at the LAAPD output were fed to a low-noise charge preamplifier (*Canberra 2004*), with a sensitivity of 45mV/MeV, to a linear amplifier (*HP 5582A*), and finally stored in a 1024-channel analyzer (*Nucleus PCA II*). The LAAPD performance was found to be optimum for 100-200 ns shaping time constants in the linear amplifier.

Figure 2 depicts the energy resolution and the minimum detectable energy (MDE) as a function of gain for LAAPD 4. The MDE is here defined as the energy corresponding to the point where the noise level rises above the background level in the pulse-height distribution, for a counting rate of about 10^3/s. Measurements were performed with a collimated X-ray beam (1 mm diameter) using 200 ns shaping time constants [16]. The best energy resolution is achieved for gains around 50 and degrades at higher gains. The same trend is observed for the

LAAPD No.	Optimum Gain	M.D.E. (keV)	E. Resolution (1 mm diameter)	E. Resolution (full area)
1	72	0.9	10.3%	12.3%
2	53	1.1	11.8%	14.9%
3	52	2.2	17.9%	18.8%
4	46	1.2	11.4%	12.3%

Table 2. Optimum performance characteristics of several LAAPDs for 5.9 keV X-rays.

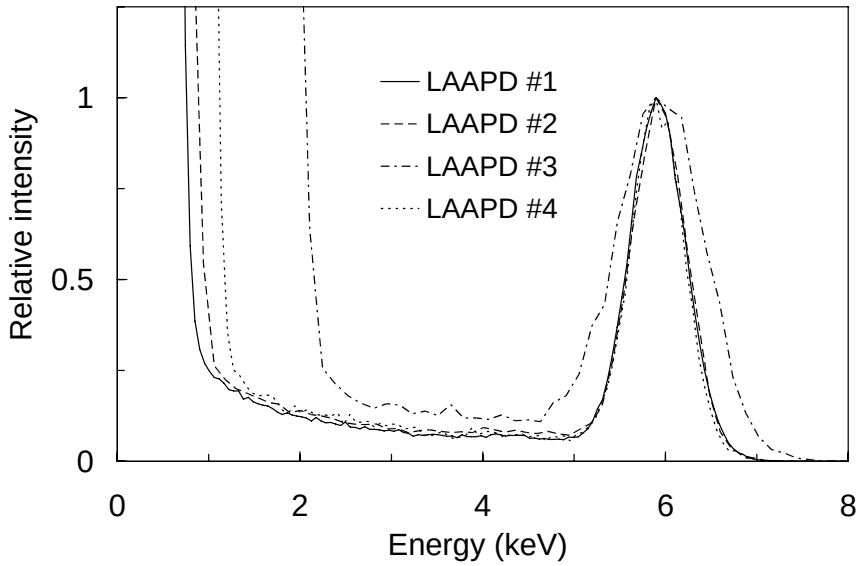

Figure 3. Typical pulse-height distributions for 5.9 keV X-rays detected by the LAAPDs described in table 1, for the optimum gain of each LAAPD.

MDE. The variation of the energy resolution for gains between 30 and 80 is very soft (between 11.4 and 12.0%), so we may conclude that the choice of the optimum gain is not critical since the APD performance does not vary significantly over a reasonable gain range.

Figure 2 presents also a calculated estimate of the energy resolution, obtained from eq. (2.11) using typical APD parameters for $\tau = 200$ ns and $T = 20$ ºC. The intrinsic resolution for 5.9 keV X-rays was obtained using eq. (2.7), F being derived from eq. (2.11) with $k_{ef} = 0.0015$, and assuming a gain non-uniformity $\sigma_U / G = 0.02$ [36]. The noise contribution was estimated using the dark current values provided by the manufacturer, which follow the equation $I_D = 24.2 + 0.64 \times G$ [nA], and taking into account the total capacitance in the preamp input, dominated by the APD (65 pF for 10 mm diameter APDs [26]), and the noise equivalent resistance in the preamplifier input, $R_{eq} \cong 33\,\Omega$.

The difference between the experimental values and the calculated estimated of the energy resolution is small for gains around the optimum but increases for higher gains. In this region, the resolution is affected by the dark current and the excess noise factor. Both were not experimentally measured here due to experimental system limitations.

Table 2 presents the optimum operational characteristics (gain, MDE and energy resolution) of each LAAPD for 5.9 keV X-rays. The energy resolution was determined both for 1 mm collimation of the X-ray beam and for full area illumination. In the first case, the best

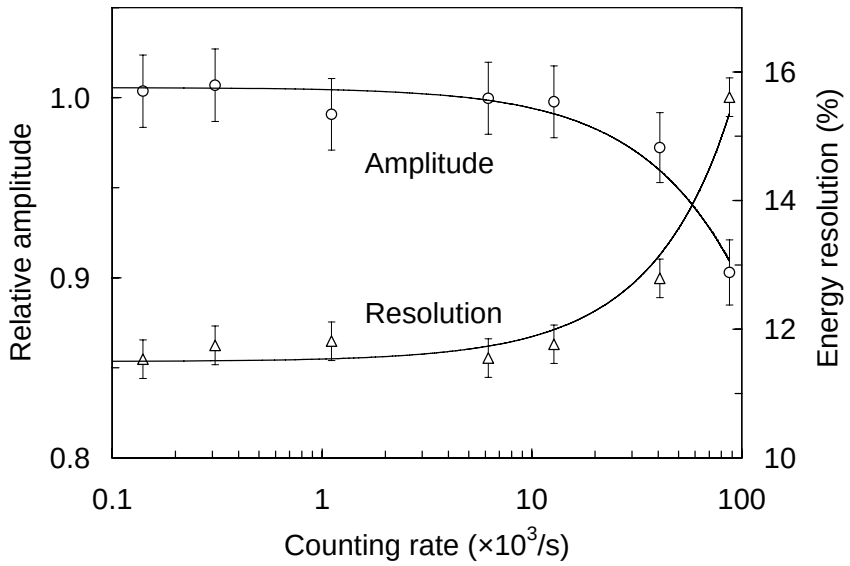

Figure 4. Relative amplitude and energy resolution for 5.9 keV X-rays as a function of the counting rate in LAAPD 4, for shaping time constants of 100 ns. The lines are exponential fits to the data.

energy resolution varies between 10 and 18% for the different LAAPDs. For full area illumination, the energy resolution is worse due to the gain non-uniformity over the device volume.

Figure 3 shows typical pulse-height distributions for 5.9 keV X-rays detected by the different LAAPDs. The X-ray peak departs from the Gaussian shape, presenting a tail towards the low energy region. This tail results from X-ray interactions in the multiplication and drift regions of the LAAPD, as described before. The correspondence between dark current (table 1) and the APD performance is clearly demonstrated in figure 3 since higher dark current values result in reduced performance for both energy resolution (peak broadening) and MDE.

Non-uniform silicon resistivity of the LAAPD results in gain fluctuations due to local electric field variations. As a result, the APD response to incident X-rays depends on their interaction position. The spatial uniformity was studied for different LAAPDs by measuring the pulse amplitude obtained for 5.9 keV X-ray collimated beams (1 mm diameter) positioned at 17 equally distributed positions over the APD area [16]. For all LAAPDs, the relative standard deviation due to non-uniformity was found to be in the 2-3% range for the optimum gain. No correlation between dark current and non-uniformity was found.

The pulse amplitude and energy resolution were investigated as a function of the counting rate. Figure 4 shows the results obtained for LAAPD 4 using shaping time constants of 100 ns. As shown, the LAAPD is able to work at counting rates as high as 10^4/s without significant amplitude and energy resolution variations. For higher counting rates, pulse pile-up takes place, distorting the peak shape and degrading the energy resolution. In addition, the pulse amplitude decreases as a result of space charge effects, as it will be shown next. For 4×10^4 counts/s, a pulse amplitude reduction of 3% and an energy resolution degradation from 12% to 13% are observed. The same trend was observed for the other LAAPDs.

Space charge effects may take place when high signal current densities are created by absorbed X-rays at high gains, resulting in electric field reduction and local heating in the avalanche region. As a result, the LAAPD response is non-linear. This effect was investigated by comparing the pulse amplitudes for 5.9 keV and 22.1 keV X-rays, emitted by ^{55}Fe and ^{109}Cd

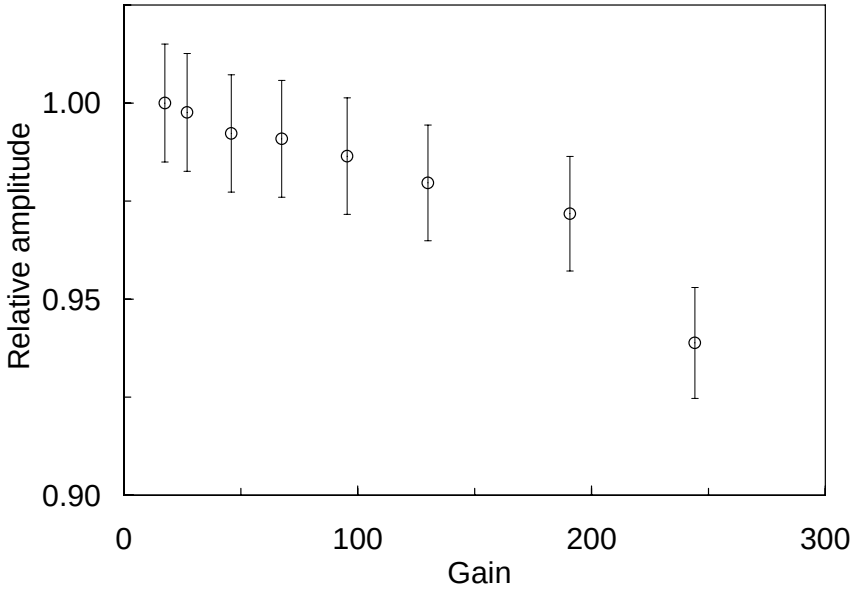

Figure 5. Relative amplitude of pulses produced in LAAPD 4 (table 1) by 22.1 keV and 5.9 keV X-rays as a function of the LAAPD gain.

radioactive sources, respectively, as a function of gain. Figure 5 shows the ratio between normalized pulse amplitudes. The ratio decreases with increasing gain. For gains up to 100 less than 1% variations are observed, while for gains of about 200 and 250, the ratio decreases by about 3% and 6%, respectively.

The LAAPD non-linearity was also investigated for higher energy X-rays using a ^{241}Am source, which emits 59.6 keV X-rays as well as 13.9 and 17.6 keV X-rays (from Np fluorescence lines, L_α and L_β). The amplitude ratio between 59.6 and 17.6 keV X-ray pulses was found to decrease with gain, reaching variations of 6, 10 and 17% for gains of 50, 100 and 200, respectively. The gain non-linearity for X-rays is more significant for higher energies since larger avalanches are created, causing higher current densities in the LAAPD.

3.2 Effect of temperature on the LAAPD gain and performance

The strong dependence of the LAAPD gain and dark current on temperature may be a drawback for many applications, requiring temperature control and stabilization during measurements. When this is not possible, temperature corrections can be made from the knowledge of the gain variation with temperature. In addition, as dark current is strongly reduced at lower temperatures the APD operation at reduced temperatures may result in improved performance [11],[13],[19],[21],[37].

The LAAPD response to X-rays was investigated as a function of temperature [21]. The gain was measured for 5.9 keV X-rays and, for the same voltage, was found to increase as temperature decreases. Figure 6 shows the gain as function of temperature for different voltages. For each bias voltage, the relative gain variation is almost constant for temperatures above -15ºC.

This is a first measurement of the variation of the LAAPD gain with temperature for X-rays; only results for visible light have been reported in the literature. For the LAAPDs investigated, the relative gain variation increases with voltage, reaching about -4% per ºC for

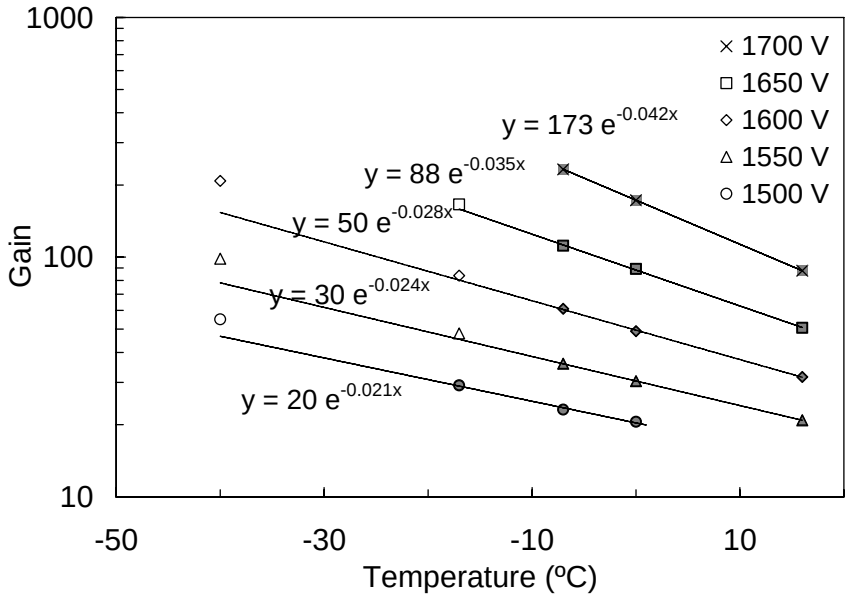

Figure 6. Gain obtained for 5.9 keV X-rays as a function of temperature, for different bias voltages applied to the LAAPD. The lines are exponential fits to the data.

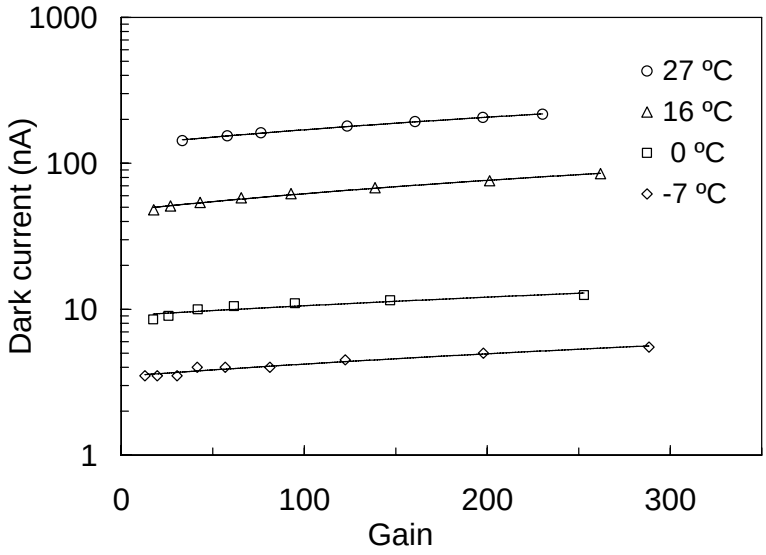

Figure 7. LAAPD dark current as a function of gain for different temperatures. The lines are linear fits to the data points.

gains above 200. These values are larger than those reported by the manufacturer for visible light, about -3% per ºC for the maximum bias voltages [26].

Figure 7 shows the LAAPD dark current as a function of gain, measured for different temperatures. The dark current varies linearly with gain, as demonstrated by the linear fits to the data shown in figure 7. For a given gain, dark current is reduced by more than one order of magnitude as the temperature is reduced from 24ºC to 0ºC.

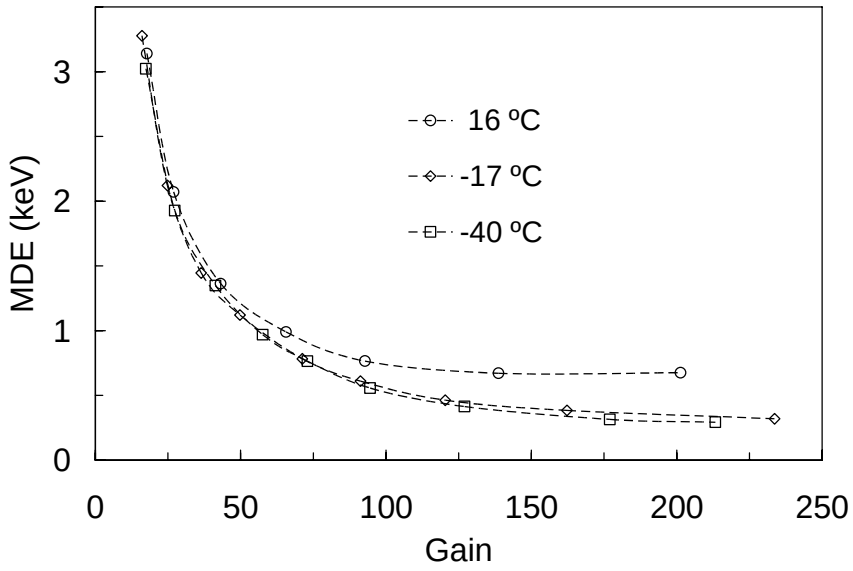

Figure 8. Minimum detectable energy as a function of gain for different temperatures.

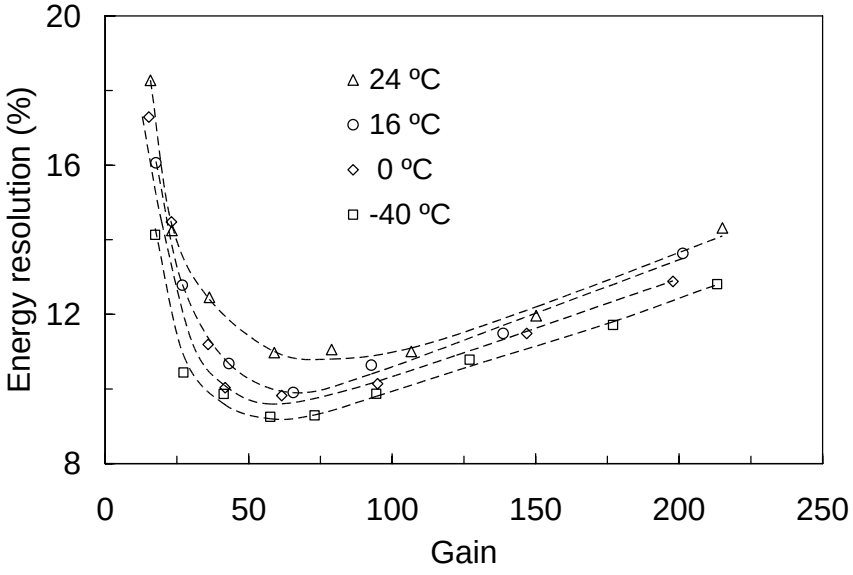

Figure 9. Energy resolution obtained for 5.9 keV X-rays as a function of gain, for different temperatures.

As dark current is a noise source, its variation with temperature affects the LAAPD performance. The MDE and energy resolution were investigated at different temperatures for full illumination of the LAAPD active area with 5.9 keV X-rays at counting rates of about 10^2/s.

Figure 8 shows the MDE as a function of gain. As shown, the MDE improves with decreasing temperature but not significantly between -17ºC and -40ºC. The MDE initially presents a fast decrease with gain, stabilizing for higher gains. Figure 8 shows that, for counting rates of 10^2/s, the LAAPD is useful for X-ray detection down to about 0.7 keV at room temperature or even down to 0.3 keV when it is cooled down to below 0ºC.

Figure 9 shows the energy resolution for 5.9 keV X-rays as a function of gain for different temperatures. As seen, the best energy resolution is obtained for gains in the range 60-80. The

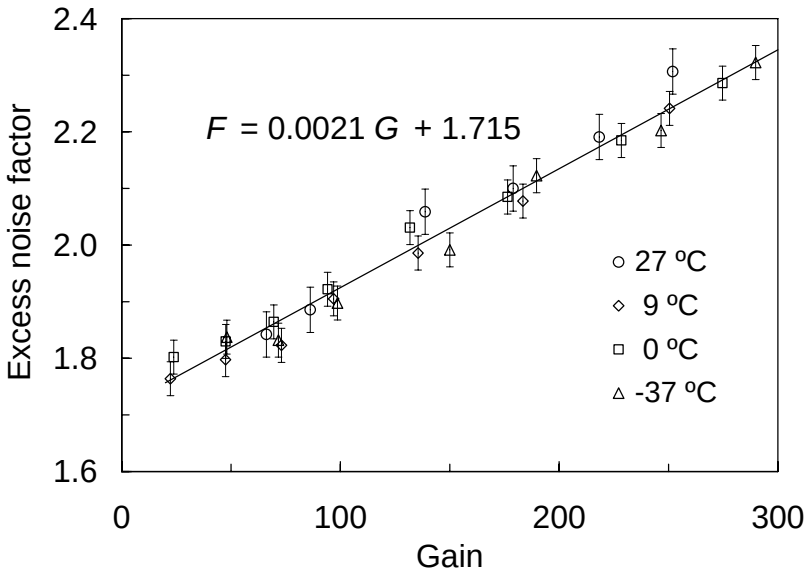

Figure 10. Excess noise factor as a function of gain for different temperatures. The line is a linear fit to all data points.

energy resolution is better than that observed in gas proportional counters and improves from 11% to 9.6% and 9.2% as temperature varies from 24ºC down to 0ºC and -40ºC, respectively. The improvement is not significant below 0ºC. This has to do with dark current, which is lower than 10 nA below 0ºC (figure 7) and its contribution to the energy resolution is not significant.

To better understand the energy resolution behaviour, another contribution inherent to the LAAPD, the excess noise factor, was measured. The method used to determine this parameter is based on the simultaneous detection of X-rays and visible-light [20]. The excess noise factor, F, is obtained from the broadening of the light peak, ΔE, which is given by (in units of energy):

$$\Delta E^2 = (2.36)^2 FE\varepsilon + \Delta E_N{}^2 \qquad (3.1)$$

where E is the energy deposited in silicon by the light pulse ($E = N\varepsilon$) and ΔE_N is the noise contribution, determined by the width of the pulses produced in the LAAPD by a pulse generator. X-rays are used as a reference to determine E.

Figure 10 presents the excess noise factor as a function of gain for different temperatures. As seen, F does not vary significantly with temperature and its dependence on gain is approximately linear. These results are concordant with previous measurements performed at room temperature [10] and liquid nitrogen temperature [38].

The energy resolution dependence on temperature (figure 9) cannot be related to F as F is practically independent of temperature. The resolution improvement with decreasing temperatures is then mainly attributed to dark current. On the other side, the energy resolution degradation at high gains is mainly due to the increase of the excess noise factor, which makes the intrinsic resolution to increase, as results from eq. (2.7).

3.3 Behaviour under intense magnetic fields

The investigation of the LAAPD performance under intense magnetic fields was made during the tests of LAAPDs as X-ray detectors for application to the muonic hydrogen Lamb shift experiment [17],[18]. Two LAAPDs were installed inside a superconducting solenoid which

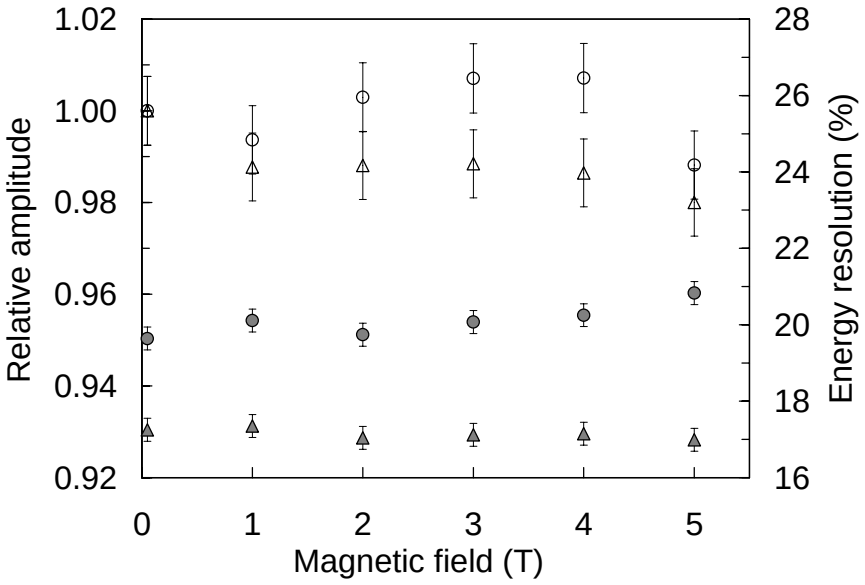

Figure 11. Relative amplitude (unfilled symbols) and energy resolution (filled simbols) of signals produced by 5.4 keV (circles) and 5.9 keV (triangles) X-rays in two LAAPDs, with axial orientations perpendicular and parallel to the magnetic field, respectively, as a function of the magnetic field intensity.

provides magnitic fields with intensities up to 5 Tesla. The LAAPDs, irradiated with ^{54}Mn and ^{55}Fe radioactive sources, were placed with different axial orientations, perpendicular and parallel to the magnetic field, respectively.

The pulse amplitude and energy resolution obtained with both LAAPDs were measured at different intensities of the magnetic field, for a bias voltage of 1800 V. Results are presented in figure 11. As shown, the relative amplitude variation with magnetic field is lower than 2% for both LAAPDs, which is within the experimental errors. The energy resolution variation is also within the experimental errors. The significant difference on the energy resolution obtained for 5.4 keV and 5.9 keV X-rays is associated not only with the energy difference but also with gain and dark current differences for the LAAPDs at the same bias voltage. The LAAPD performance is not significantly affected by magnetic fields up to 5 T, independent of the relative orientation of the electric and magnetic fields.

The LAAPD response was also investigated for X-rays with lower energy using a sulphur sample irradiated with a ^{55}Fe source [18]. The relative amplitude of the signal produced by 2.3 keV sulphur characteristic K-fluorescence X-rays was found to decrease by less than 3% when the magnetic field increased from 0 to 5 T, while the energy resolution varied between 30.5% and 32.5%. Both variations are approximately equal to the experimental errors. We conclude that LAAPDs can operate under intense magnetic fields up to 5 T without significant performance degradation for X-rays with energy as low as 2.3 keV.

3.4 X-ray spectrometry applications

The application of LAAPDs as direct X-ray detectors for X-ray spectrometry was investigated at room and lower temperatures by detecting characteristic X-rays of several samples irradiated with ^{55}Fe and ^{109}Cd radioactive sources.

The LAAPD energy linearity was investigated at room temperature for X-ray energies between 1.7 and 25 keV using the fluorescence radiation induced in single-element samples and

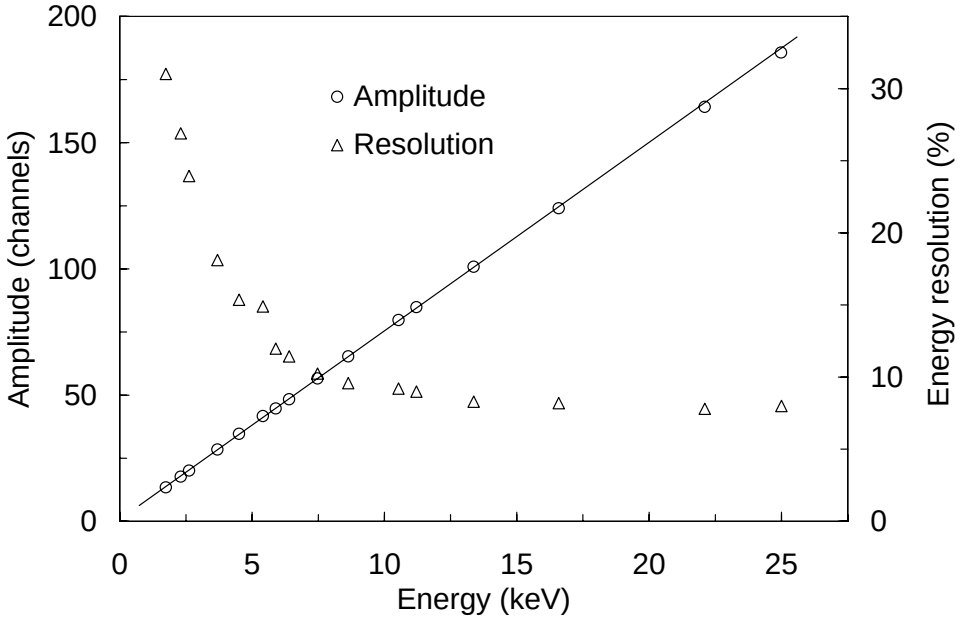

Figure 12. LAAPD pulse amplitude (peak centroid) and energy resolution as a function of the X-ray energy. A linear fit to the amplitude measurements is shown. The experimental uncertainties fall within the symbol size.

direct X-rays emitted by the radioactive sources. The LAAPD was operated at the optimum gain (around 50) with signal counting rates of 10^3 to 10^4/s. Figure 12 shows the pulse amplitude and energy resolution of X-ray peaks as a function of the X-ray energy. Good linearity is observed throughout the energy range for the optimum gain. For higher gains, non-linearity effects would take place, affecting the energy linearity.

The energy resolution decreases with increasing energy, but does not scale as $E^{-1/2}$ (E being the X-ray energy), especially for higher energies, as is the case in proportional counters. This is due to peak distortions resulting from an increasing number of X-ray interactions in the multiplication region as the energy increases.

X-ray fluorescence spectra were obtained for thick samples of gypsum ($CaSO_4$) and *SAES St707* getters (70% Zr, 5.4% Fe and 24.6% V), irradiated with ^{55}Fe and ^{109}Cd sources, as shown in figure 13(a) and (b), respectively. The distributions include the characteristic X-ray fluorescence K-lines of the sample elements as well as the backscattering radiation from the sources (Mn and Ag K-lines). Pb L-lines from the source shielding and collimator are also shown in figure 13(b). The amplitude spectra and energy resolutions are similar to those achieved with conventional proportional counters.

The previous results demonstrate the applicability of LAAPDs, working at room temperature, to energy-dispersive X-ray fluorescence analysis. Compared to gas proportional counters, LAAPDs are more compact and devices with lower dark current may achieve improved energy resolution for X-ray energies from a few keV up to about 20 keV. Its windowless feature may be crucial for detection of soft X-rays and its superior counting rate capability may be important for high counting rate applications. The LAAPD cost, limited area, limited detection efficiency for medium and high energy X-rays, as well as the sensitivity to light and temperature, are drawbacks compared to proportional counters.

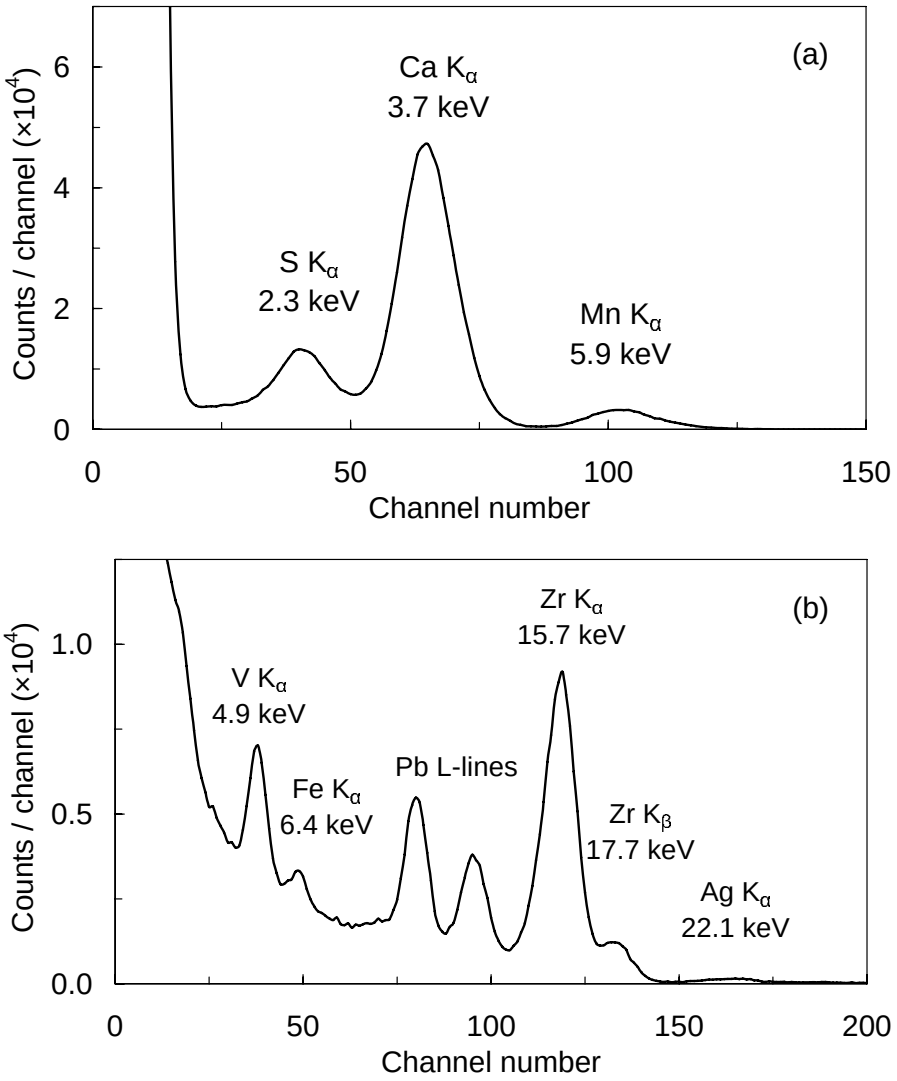

Figure 13. X-ray fluorescence spectra obtained at room temperature for two thick samples: (a) gypsum ($CaSO_4$) irradiated with a ^{55}Fe source; (b) *SAES St707* getters (70% Zr, 5.4% Fe and 24.6% V) irradiated with a ^{109}Cd source.

The applicability of LAAPDs to X-ray fluorescence analysis was investigated at different temperatures. Good energy linearity was demonstrated for energies below 20 keV for a gain of 130, independent of temperature [19]. The energy resolution improves with decreasing temperatures due to the dark current drop.

Figure 14 shows typical pulse-height distributions obtained for fluorescence X-rays from a sulphur sample irradiated with a ^{55}Fe source, for different temperatures. The distributions also include the Mn-backscattered line from the X-ray source. Gains of about 240, 280 and 320 were used for temperatures of 25, 15 and 5ºC, respectively. The energy spectra are better than those obtained with a conventional proportional counter, especially at lower temperatures. The energy resolution for 2.3 keV X-rays (S K_α-line) improves from 30 to 23% as the temperature decreases from 25 to 5ºC and the minimum detectable energy improves from 1.7 to 1.1 keV.

The advantages of the LAAPD cooling are evidenced by the obtained energy spectra through electronic noise reduction and energy resolution improvement for decreasing temperatures. As

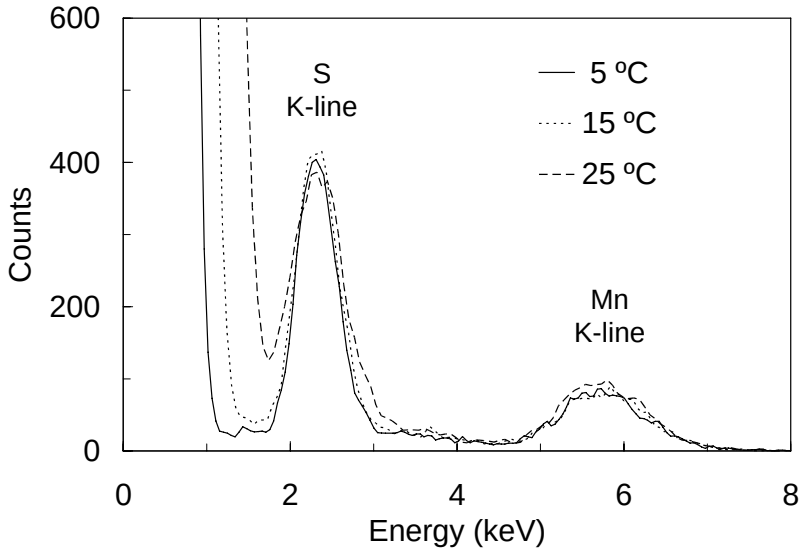

Figure 14. Pulse-height distributions for fluorescence X-rays from a sulphur sample irradiated with a ^{55}Fe source, for different operation temperatures.

shown before, below 0ºC only a small improvement is observed as the dark current contribution to the energy resolution is small. The effect of the temperature reduction is more significant for fluorescence X-rays with lower energies due to the proximity between signal and noise.

The X-ray detection in a LAAPD originates spectral peaks with tails towards lower energies and pulses with different time responses due to X-ray interactions in different regions of the APD. Digital discrimination techniques, based on pulse rise-time, demonstrated to be useful in improving the peak-to-background ratio by eliminating pulses with smaller amplitude which undergo partial amplification in the LAAPD [39]. This is important for X-ray spectrometru applications where several X-ray lines are observed and peaks with lower energy superimpose on the background of higher energy lines. In addition, noise pulses present longer rise-times and can be efficiently discriminated against signals. Nevertheless, a compromise between the acquisition efficiency of the X-ray pulses and the noise discrimination threshold is necessary as lower discrimination levels cause more dead time. Even so, the improvement from time discrimination is not so significant when compared with the device to device performance variation.

4. VUV-light detection

Avalanche photodiodes have been used in photon detection applications, where they compete favourably with photomultiplier tubes. Deep-UV windowless APDs have been investigated as photosensors for the secondary scintillation light produced in noble gases [7],[8] and liquids [40],[41] for X-ray and γ-ray spectroscopy applications. This type of APD is particularly sensitive in the VUV spectral region down to 120 nm. The emission spectrum for argon and xenon electro-lumine-scence is a narrow continuum peaking at 128 nm and 172 nm, respectively, with 10 nm FWHM for both cases [42]. The effective quantum efficiency, here defined as the average number of primary electrons produced in the APD per incident photon, is about 0.5 and 1.05 for 128 nm and 172 nm VUV light, respectively, corresponding to spectral sensitivities of 50 and 150 mA/W [43].

The use of LAAPDs as VUV photosensors in Gas Proportional Scintillation Counters (GPSCs) has shown several advantages against PMTs: compact structure, low power consump-

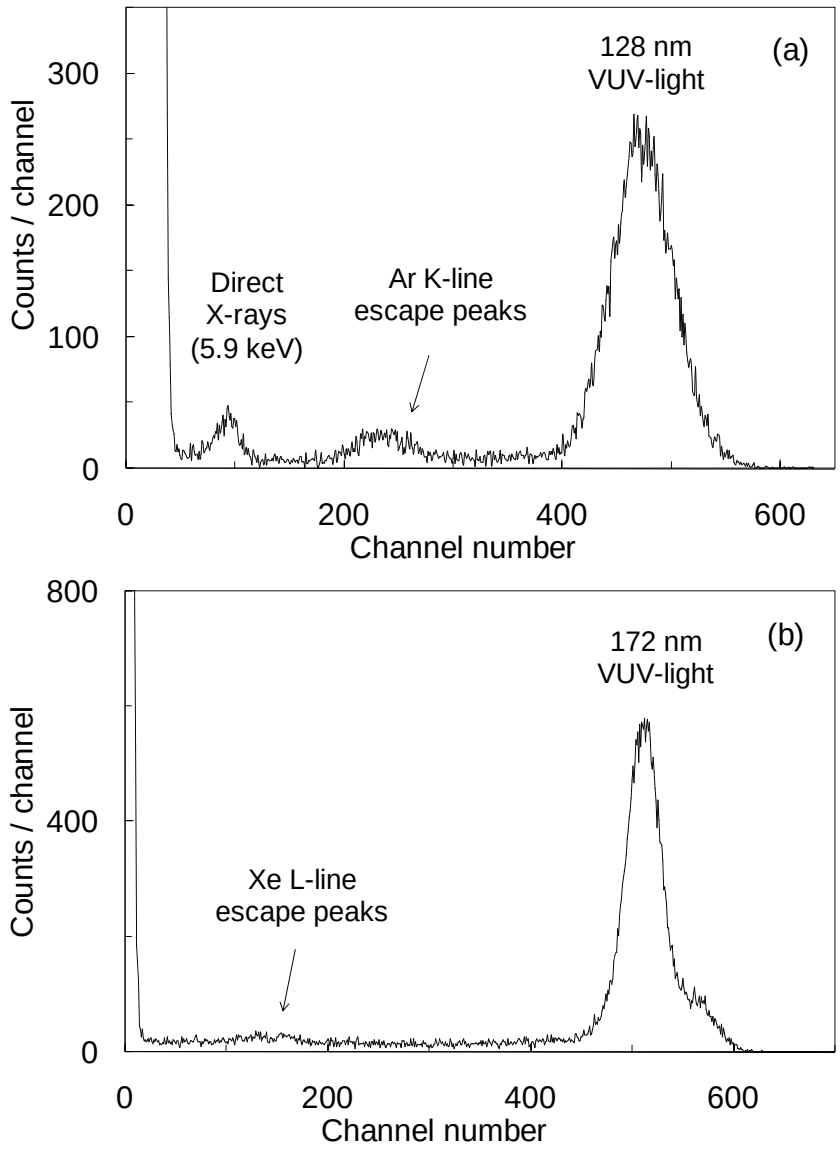

Figure 16. Typical pulse-height distributions obtained with the detector of Fig. 15 irradiated with a ^{55}Fe source and filled with argon (a) and xenon (b). The LAAPD was operated at gains of about 40 and 60 in (a) and (b), respectively.

GPSC has a 2.5 cm deep absorption (or drift) region and a 0.8 cm deep scintillation region. The entrance window (6 μm thick *Melinex*) and grid G1 are operated with negative voltages, while grid G2 is maintained at ground, in order to create appropriate electric fields in the drift and scintillation regions. The detector was filled with gas, either pure argon at 1140 Torr or pure xenon at 825 Torr, continuously purified by convection through non-evaporable getters (*SAES St707*).

Detailed theory and operation of GPSCs are described in refs. [44]-[46]. X-rays entering the GPSC window are mostly absorbed in the drift region, producing a cloud of primary electrons that drift toward the scintillation region by influence of a weak electric field. In the scintillation region, each primary electron is accelerated by a stronger electric field, exciting the gas without further ionization, and producing a VUV-light pulse (called electroluminescence or secondary scintil-

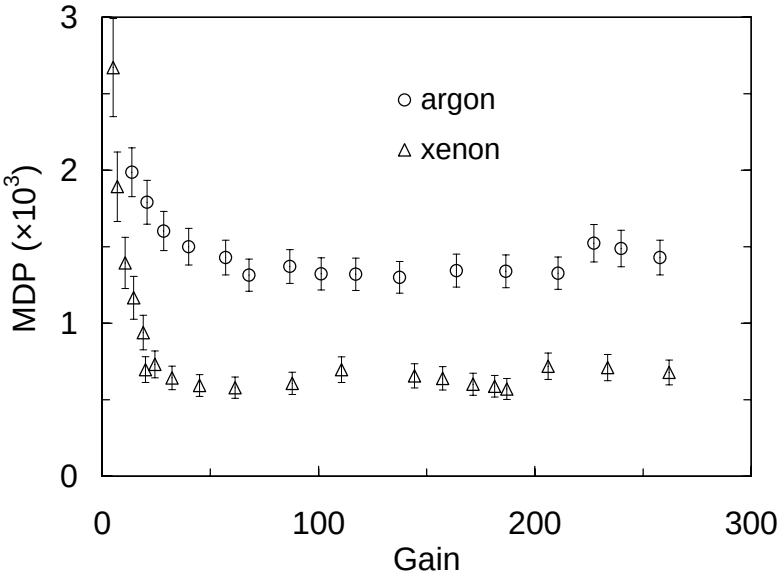

Figure 17. Minimum number of detectable photons in the LAAPD as a function of gain, for argon and xenon scintillation (around 128 nm and 172 nm, respectively).

lation) with duration of about 1 μs. Following the incidence of the VUV photons on the LAAPD, charge multiplication will take place within the LAAPD volume, creating the final signal.

The LAAPD response to the VUV light from argon and xenon electroluminescence was investigated by irradiating the GPSC with a ^{55}Fe X-ray source. LAAPD signals were fed through a low-noise charge-sensitive preamplifier (*Canberra 2006*) to a linear amplifier (*HP 5582A*) with 2 μs shaping constants and pulse-height analized.

Figure 16 shows typical pulse-height distributions for argon (a) and xenon (b). In (a), only 5.9 keV X-rays (Mn K_α line) interact in the gas since the K_β line was absorbed in a chromium foil. Under the GPSC operation conditions, each 5.9 keV X-ray absorbed in the GPSC drift region produces an average number of 7.5×10^4 and 1.2×10^5 VUV photons in argon and xenon, respectively [7],[8]. Taking into account that the average relative solid angle subtended by the LAAPD is approximately 0.2 [47], the number of VUV photons that hit the APD active area is about 1.5×10^4 and 2.5×10^4 for argon and xenon scintillation, respectively.

The main features of the pulse-height distributions include the scintillation peaks resulting from the full absorption of X-rays in the gas and subsequent gas fluorescence escape peaks, as well as the electronic noise tail. In (a), there is an additional peak resulting from direct absorption of 5.9 keV X-rays in the LAAPD. Approximately 10% of these X-rays are transmitted through the argon (3.3 cm depth). In (b), this does not happen because the absorption of 5.9 keV X-rays in xenon is practically 100% and no X-rays reach the LAAPD area.

In argon, the peak resulting from 5.9 keV X-rays directly absorbed in the LAAPD can be used as a reference to determine the number of charge carriers produced by the VUV-light pulse. The charge deposited in silicon by the argon scintillation pulse is equivalent to that produced by a 30 keV X-ray photon and so the number of primary electrons produced in the LAAPD is $N = 8 \times 10^3$. This is consistent with the LAAPD quantum efficiency of 50% for argon scintillation [48] as the number of VUV photons that hit the APD is 1.5×10^4.

The LAAPD gain for argon and xenon scintillation was determined as a function of bias voltage and its performance was investigated as a function of gain. Figure 17 shows the

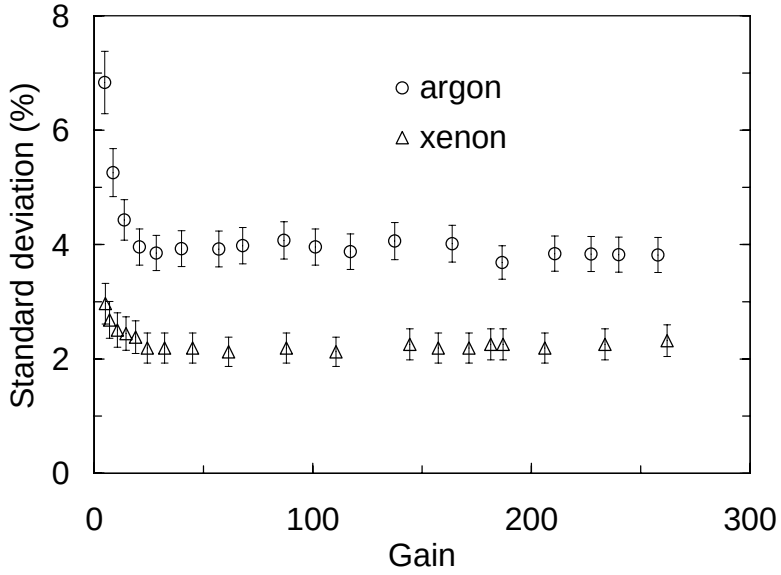

Figure 18. Relative standard deviation associated with the detection of VUV photons, 1.5×10^4 in argon (~128 nm) and 2.5×10^4 in xenon (~172 nm), as a function of the LAAPD gain.

Minimum number of Detectable Photons (MDP) for argon and xenon scintillation, here defined as the number of photons that would produce a LAAPD signal with an amplitude corresponding to the point where the electronic noise tail in the pulse-height distribution rises above the signal background level. The MDP variation with gain shows a similar trend for both argon and xenon scintillation. For low gains, the MDP decreases significantly as the gain drops, stabilizing in about 1300 and 600 photons for gains above 60 (in argon) and 40 (in xenon), respectively. The MDP for 172 nm VUV light is about half of that for 128 nm VUV light, reflecting the ratio between the LAAPD quantum efficiencies for those wavelengths [48].

The statistical fluctuations associated with VUV-photon detection in the LAAPD can be estimated from the energy resolution measured for the scintillation peaks. The energy resolution of the GPSC is given by [46]:

$$R = 2.355\sqrt{\frac{f\,w}{E_x} + \left(\frac{\Delta E}{E}\right)^2} \tag{4.1}$$

E_x being the energy of incident X-rays (5.9 keV), f the Fano factor (0.30 for argon and 0.17 for xenon [50]), w the average energy required to create a primary electron in the gas (26.4 eV for argon [29] and 22.4 eV for xenon [49]) and E the energy deposited in the photosensor by the VUV scintillation pulse. $\Delta E/E$ represents the statistical fluctuations associated to the VUV photon detection, i.e. the photossensor contribution (relative standard deviation) to the GPSC energy resolution.

Figure 18 shows the relative standard deviation associated with the detection of VUV photons (1.5×10^4 in argon and 2.5×10^4 in xenon) as a function of the LAAPD gain. The relative uncertainty decreases rapidly with the onset of gain and stabilizes for gains above 30, reaching 3.9% and 2.2% for argon and xenon scintillation, respectively.

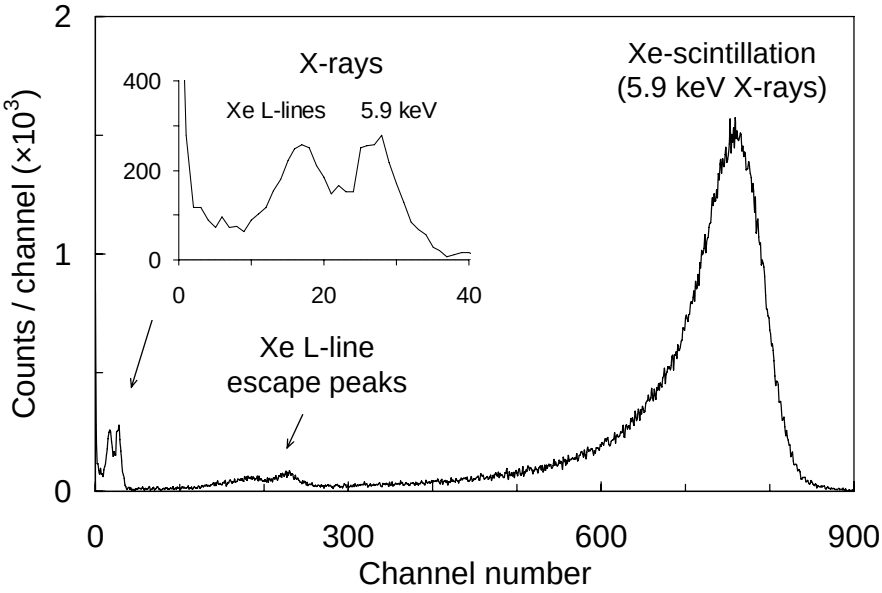

Figure 19. Pulse-height distribution of LAAPD pulses resulting from 5.9 keV X-rays interacting in the driftless GPSC. The LAAPD was operated at a gain of 100.

As shown in figure 18, a gain as low as 30 is sufficient to achieve the best response of the LAAPD. For low light levels, higher gains will be needed to separate the light pulse from the noise and achieve the best performance.

The minimum number of detectable photons and the statistical fluctuations associated with VUV-light detection do not depend directly on the photon wavelength, but rather on the number of charge carriers produced by the light pulse in the LAAPD.

4.2 Non-linearity between gains for X-rays and VUV light

The non-linearity study requires the comparison of the amplitude of signals produced by X-rays directly absorbed in the LAAPD and those resulting from the scintillation light produced in the gas. Using the detector of figure 15, this study is possible only for argon as a fraction of the X-rays are transmitted through the gas and absorbed in the LAAPD. For xenon, as the X-ray transmission is much lower, the non-linearity study was performed with a different GPSC, made without drift region. This driftless GPSC has a 1.1 cm deep scintillation region, where about 0.2% of X-rays are transmitted through the gas, interacting directly in the LAAPD.

In the driftless GPSC, the total number of scintillation photons produced by primary electrons accelerated through the electric field depends on how deep the X-ray absorption takes place. As a result, the driftless design results in worse energy resolution. Figure 19 shows a typical pulse-height distribution obtained from 5.9 keV X-rays interacting in the driftless GPSC. The scintillation peak is asymmetric and presents larger energy resolution than that of figure 16(b). In addition to the scintillation peaks, the peaks resulting from direct X-ray absorptions in the LAAPD are also visible. These include 5.9 keV X-rays from the ^{55}Fe source and xenon fluorescence X-rays (4.1 keV and 4.4 keV from L_α and L_β lines).

The LAAPD gain was determined from amplitude measurements for VUV-light pulses and unitary gain was found at a bias voltage of 500V. The gain for X-rays was determined by normalization to VUV-light measurements at the lowest gain where X-ray signals are correctly detected. At this gain (~10), space charge effects are negligible and the gain measurement for

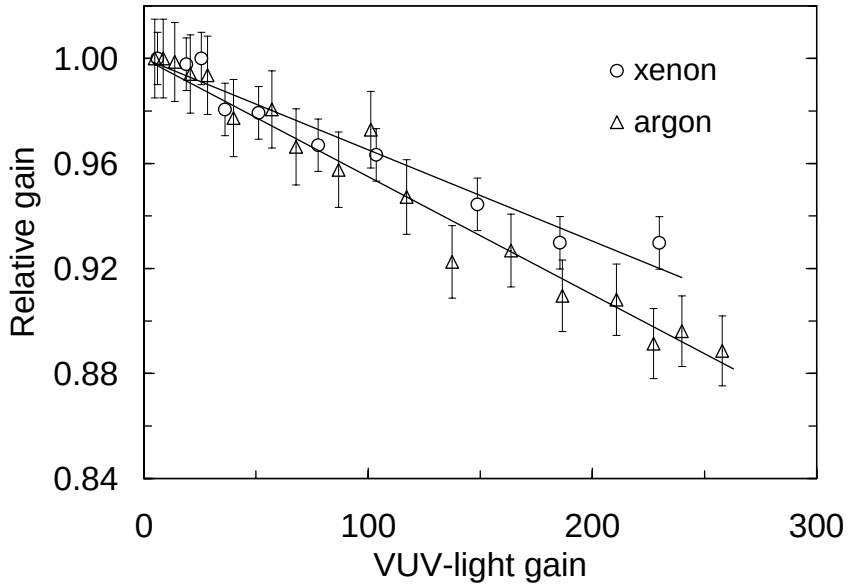

Figure 20. LAAPD relative gain for 5.9 keV X-rays and VUV light from argon and xenon scintillation, as a function of the LAAPD gain measured with VUV light.

X-rays is not compromised. Figure 20 shows the relative gain for 5.9 keV X-rays and VUV-light pulses produced in argon and xenon as a function of the gain measured with VUV light. The variation is approximately linear and reaches about -7% and -10% for xenon and argon, respectively, at a gain of 200.

The non-linearity study was extended to X-rays with higher energy. For 22.1 keV X-rays interacting in the xenon GPSC, the X-ray to VUV-light gain ratio presents variations significantly higher than those obtained with 5.9 keV X-rays, reaching -13% for a gain of 200. This results from further space charge effects for X-rays with higher energy and is consistent with the trend shown in figure 5.

In addition to space charge effects resulting from the point-like nature of X-ray interactions, the previous results suggest a wavelength dependence of the discrepancy between X-ray and VUV light gains. The discrepancy is higher for 128 nm than for 172 nm VUV photons and both are higher than that reported for visible light (~600 nm) [25]. The non-linearity must depend on the penetration depth in silicon for each photon. VUV and visible light photons are absorbed in the drift region of the LAAPD, where the electric field is very weak and the effect of electron capture is more significant. As the absorption is much more superficial for VUV light (~5 nm), capture is greater in this case but decreases with gain due to the corresponding electric field increase. Thus, the higher LAAPD voltage helps to collect charges produced near the entrance surface. This effect is smaller for xenon than for argon and probably negligible for visible light, which has much larger penetration depth.

An accurate determination of the number of charge carriers produced in the LAAPD by VUV-light photons using X-rays as a reference must take into account the discrepancies described above. This is especially the case for high LAAPD gains.

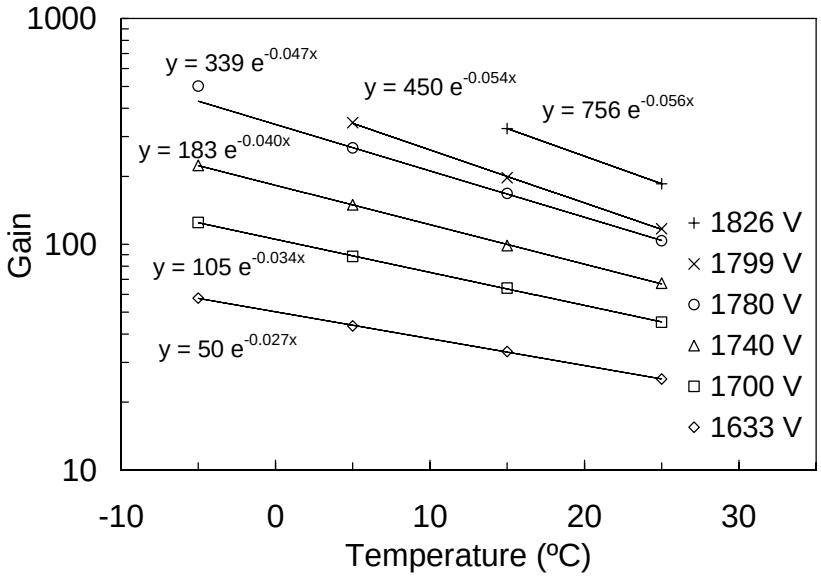

Figure 21. LAAPD gain measured for xenon scintillation light (~172 nm) as a function of temperature for different bias voltages. The lines are exponential fits to the data.

4.3 Temperature dependence

The LAAPD response to VUV-light was investigated as a function of temperature using a LAAPD with an integrated Peltier cell (*571 cooled head series* from API) incorporated in a xenon GPSC with 3.1 and 0.9 cm thick absorption and scintillation regions, respectively, irradiated with 5.9 keV X-rays. Under the experimental conditions, each X-ray absorbed in the drift region creates about 1.35×10^5 VUV photons. Taking into account the relative solid angle of 0.2 subtended by the LAAPD [7], about 2.7×10^4 VUV photons are detected in the LAAPD per X-ray interaction in the gas.

The gain was determined from the amplitude distributions obtained for different temperatures and was found to increase with decreasing temperature. The maximum achievable gain increases from 300 to more than 700 as temperature decreases from 25 to -5 ºC [24]. Figure 21 shows the LAAPD gain measured for xenon scintillation light as a function of temperature for different bias voltages. Exponential fits to the data are shown. For each voltage, the relative gain variation is almost constant and increases from -2.7% to -5.6% per ºC as the voltage increases from 1633 to 1826 V. For gains above 200, the relative gain variations are almost a factor of 2 higher than those reported for visible light, about -3% per ºC [26].

The minimum number of detectable photons (MDP) and the energy resolution for xenon scintillation were also determined for different temperatures and the statistical fluctuations associated to VUV-light detection were estimated from eq. (4.1). The MDP was found to stabilize for gains above 100 and improves as the LAAPD temperature varies from 25 ºC down to 5ºC. The minimum statistical fluctuations of the LAAPD were achieved for gains around 100, which do not depend significantly of temperature.

4.4 Behaviour under intense magnetic fields

The insensitivity of avalanche photodiodes to magnetic fields has often been referred to in the literature [2],[27] but detailed experimental results are scarce. Most of the studies were carried

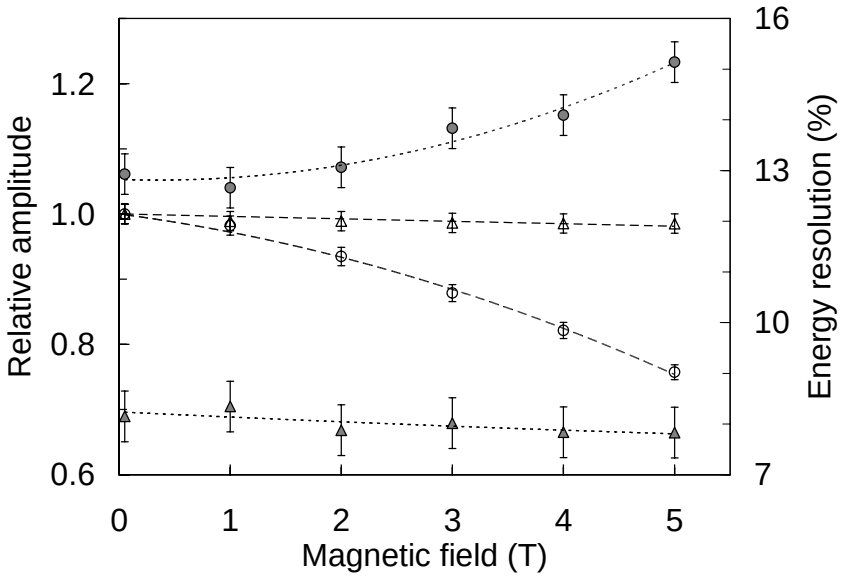

Figure 22. Relative pulse amplitude (unfilled symbols) and energy resolution (filled symbols) as a function of the magnetic field intensity, for visible light (triangles) and xenon VUV light (circles).

out for visible light and only for magnetic field intensities of a few Tesla. The behaviour of LAAPDs under magnetic fields up to 5 T was investigated for VUV-light detection using the driftless GPSC previously described irradiated with a collimated X-ray beam from a ^{55}Fe source. For comparison and because some LAAPD characteristics are different for visible and VUV light, the APD response to visible light was also investigated. A cubic CsI (Tl) crystal was irradiated with 835 keV γ-rays from a ^{54}Mn radioactive source and the scintillation light (~520 nm) produced by each γ-ray interaction was detected by a LAAPD. The LAAPD was operated at 1800 V in both cases and shaping time constants of 1 and 2 μs were used in the linear amplifier for visible and VUV light measurements, respectively.

The pulse-height distributions obtained for visible light include a peak resulting from full energy absorption of γ-rays in the crystal, a Compton continuum and the electronic noise tail. Pulse-height distributions for VUV light are similar to that shown in figure 19. Figure 22 shows the relative amplitude and energy resolution for LAAPD signals produced by CsI(Tl) scintillation visible light and xenon scintillation VUV light as a function of the magnetic field. For visible light, amplitude variations are within the experimental errors (± 1%) and no significant energy resolution variations are observed. For VUV light, the relative amplitude decreases gradually as the magnetic field increases, reaching a 24% variation at 5 T, while an energy resolution degradation from 13% to 15% is observed.

The effect of magnetic field on the GPSC scintillation and possible variations of the solid angle subtended by the LAAPD due to the Lorentz angle are negligible [51]. Thus, the noticeable influence of the magnetic field in VUV-light detection has its origin in the LAAPD. As VUV photons interact within the first few atomic layers of silicon, where the electric field is weaker, the magnetic field affects the produced photoelectrons and the diffusion of secondary electrons, causing partial charge loss to the dead layer in the LAAPD entrance.

5. Conclusions

We have investigated in detail the response characteristics of API large area avalanche photodiodes for X-ray and VUV-light detection. These studies have shown that LAAPDs can be used for X-ray detection for energies up to about 25 keV, being robust detectors with simple operation and very low power consumption. These characteristics make them particularly useful in X-ray spectrometry applications.

The operational characteristics of several LAAPDs in X-ray detection were determined at room temperature. The APD performance depends significantly on each individual device since the dark current varies significantly among different LAAPDs. For the four studied LAAPDs, the best energy resolution obtained for 5.9 keV X-rays varies between 10 and 18% range. The minimum detectable energy may be lower than 1 keV for LAAPDs with inferior dark current. LAAPDs with low dark current are preferred since an energy resolution better than that of typical proportional counters can be obtained. The LAAPD compact structure, windowless design, high counting rate capability (more than 10^4/s without performance degradation) and insensitivity to intense magnetic fields (up to 5 Tesla) are additional advantages. In contrast, the limited area and sensitivity to light and temperature are drawbacks.

The energy linearity of LAAPDs in X-ray detection was demonstrated for energies between 1.7 and 25 keV around the optimum gain. There is however a small effect of non-linearity for higher gains, resulting from space charge effects associated with the local absorption of X-rays. Another consequence of the point-like absorption of X-rays is the fluctuation of the LAAPD gain due to the non-uniformity of the silicon resistivity. Relative standard deviations of 2-3% in the gain of API LAAPDS were measured as a result of the non-uniformity effect.

The LAAPD gain and dark current depend strongly on temperature, limiting the LAAPD response in X-ray detection. For 5.9 keV X-rays, the relative gain variation with temperature is more than -4% per ºC for the highest gains. The LAAPD energy resolution and minimum detectable energy improve with decreasing temperatures down to 0ºC due to the significant dark current reduction. Below 0ºC, the dark current contribution to energy resolution is low and no significant improvement of the LAAPD performance is observed. For a LAAPD investigated, the best energy resolution measured for 5.9 keV X-rays is 11.0, 9.6 and 9.2% for temperatures of 24, 0 and -40 ºC. The excess noise factor was determined and found to be independent of temperature, confirming that the energy resolution dependence on temperature cannot be attributed to the excess noise factor, being mainly determined by the dark current. The linear dependence of the excess noise factor on the LAAPD gain is responsible for the energy resolution degradation at higher gains.

LAAPDs were also investigated as VUV photosensors in gas proportional scintillation counters. The relative gain variation with temperature for the VUV light is somewhat higher than the one observed for X-rays. As a result of the dark current variation with temperature, both the minimum detection limit and energy resolution improve with decreasing temperature. The LAAPD response in VUV-light was found to vary significantly under intense magnetic fields, opposite to the response in X-ray detection. This different behaviour is due to the superficial absorption of VUV photons, causing partial loss of primary electrons to the dead layer in the APD entrance.

The number of electron-hole pairs produced in the LAAPD by light pulses is often determined using X-rays as a reference. This is affected by the gain difference for X-rays and light signals. The LAAPD non-linearity for X-rays and VUV-light pulses was investigated for

the first time. The gain ratio between 5.9 keV X-rays and VUV light was found to decrease with gain. For a gain 200, about 10 and 6% variations were obtained for the argon (~128 nm) and xenon (~172 nm) scintillation, respectively. These variations are much larger than that observed between 5.9 keV X-rays and visible light (less those 1% for a gain of 200).

Acknowledgments

The work was mostly carried out in the Atomic and Nuclear Instrumentation Group of the Instrumentation Centre (Research Unit 217/94) of the Physics Department, University of Coimbra, and received support from Swiss National Science Foundation and Fundação para a Ciência e a Tecnologia (FCT), Portugal, through FEDER and POCI2010 programs, projects POCTI/FIS/13140/98, POCTI/FNU/41720/01, CERN/FIS/43785/01 and POCI/FIS/60534/2004.

L.M.P. Fernandes acknowledges grant from FCT (Ref. SFRH/BD/5426/2001).

References

[1] R. Farrell, F. Olschner, K. Shah and M.R. Squillante, *Advances in semiconductor photodetectors for scintillation*, *Nucl. Instrum. Meth.* **A 387** (1997) 194.

[2] A. Karar, Y. Musienko and J.Ch. Vanel, *Characterization of avalanche photodiodes for calorimetry applications*, *Nucl. Instrum. Meth.* **A 428** (1999) 413.

[3] K. Deiters et al., *Properties of the most recent avalanche photodiodes for the CMS electromagnetic calorimeter*, *Nucl. Instrum. Meth.* **A 442** (2000) 193.

[4] M. Moszynski, M. Szawlowsky, M. Kapusta and M. Balcerzyk, *Avalanche photodiodes in scintillation detection*, *Nucl. Instrum. Meth.* **A 497** (2003) 226.

[5] B. Pichler et al., *Studies with a prototype high resolution PET scanner based on LSO-APD modules*, *IEEE Trans. Nucl. Sci.* **45** (1998) 1298.

[6] A. Ruru Chen et al., *Readout of scintillator light with avalanche photodiodes for positron emission tomography*, *Nucl. Instrum. Meth.* **A 433** (1999) 637.

[7] J.A.M. Lopes, J.M.F. dos Santos, R.E. Morgado and C.A.N. Conde, *A xenon gas proportional scintillation counter with a UV-sensitive large-area avalanche photodiode*, *IEEE Trans. Nucl. Sci.* **48** (2001) 312.

[8] C.M.B. Monteiro, J.A.M. Lopes, P.C.P.S. Simões, J.M.F. dos Santos and C.A.N. Conde, *An argon gas proportional scintillation counter with UV avalanche photodiode scintillation readout*, *IEEE Trans. Nucl. Sci.* **48** (2001) 1081.

[9] E.M. Gullikson, E. Gramsch and M. Szawlowski, *Large-area avalanche photodiodes for the detection of soft X-rays*, *Appl. Optics* **34** (1995) 4662.

[10] M. Moszynski, M. Szawlowski, M. Kapusta, M. Balcerzyk and D. Wolski, *Large avalanche photodiodes in X-rays and scintillation detection*, *Nucl. Instrum. Meth.* **A 442** (2000) 230.

[11] R. Farrell, K. Vanderpuye, G. Entine and M.R. Squillante, *High resolution, low energy avalanche photodiode X-ray detectors*, *IEEE Trans. Nucl. Sci.* **38** (1991) 144.

[12] P.P. Webb and R.J. McIntyre, *Large area reach-through avalanche diodes for X-ray spectroscopy*, *IEEE Trans. Nucl. Sci.* **23** (1976) 138.

[13] A. Ochi, Y. Nishi and T. Tanimori, *Study of a large area avalanche photodiode as a fast photon and a soft X-ray detector*, *Nucl. Instrum. Meth.* **A 378** (1996) 267.

[14] J.P. Pansart, *Avalanche photodiodes for particle detection*, *Nucl. Instrum. Meth.* **A 387** (1997) 186.

[15] C.P. Allier, H. Valk, J. Huizenga, V.R. Bom, R.W. Hollander and C.W.E van Eijk, *Comparative study of silicon detectors*, *IEEE Trans. Nucl. Sci.* **45** (1998) 576.

[16] L.M.P. Fernandes, J.A.M. Lopes, J..F. dos Santos and C.A.N. Conde, *Application of large area avalanche photodiodes to energy dispersive X-ray fluorescence analysis*, *X-ray Spectrom.* **30** (2001) 164.

[17] L.M.P. Fernandes et al., *Behaviour of large-area avalanche photodiodes under intense magnetic fields for VUV, visible and X-ray photon detection*, *Nucl. Instrum. Meth.* **A 498** (2003) 362.

[18] M. Boucher et al., *Large-area APDs for low-energy X-ray detection in intense magnetic fields*, *Nucl. Instrum. Meth.* **A 505** (2003) 136.

[19] L.M.P. Fernandes, J.A.M. Lopes, J.M.F. dos Santos and C.A.N. Conde, *X-ray spectrometry with Peltier-cooled large area avalanche photodiodes*, *Nucl. Instrum. Meth.* **B 213** (2004) 267.

[20] L.M.P. Fernandes, J.A.M. Lopes and J.M.F. dos Santos, *Excess noise factor in large area avalanche photodiodes for different temperatures*, *Nucl. Instrum. Meth.* **A 531** (2004) 566.

[21] L.M.P. Fernandes et al., *LAAPD low temperature performance in X-ray and visible-light detection*, *IEEE Trans. Nucl. Sci.* **51** (2004) 1575.

[22] J.A.M. Lopes, J.M.F. dos Santos and C.A.N. Conde, *A large area avalanche photodiode as the VUV photosensor for gas proportional scintillation counters*, *Nucl. Instrum. Meth.* **A 454** (2000) 421.

[23] L.M.P. Fernandes, J.A.M. Lopes, C.M.B. Monteiro, J.M.F. dos Santos and R.E. Morgado, *Non-linear behaviour of large-area avalanche photodiodes*, *Nucl. Instrum. Meth.* **A 478** (2000) 395.

[24] J.A.M. Lopes, L.M.P. Fernandes, J.M.F. dos Santos, R.E. Morgado and C.A.N. Conde, *VUV detection in large-area avalanche photodiodes as a function of temperature*, *Nucl. Instrum. Meth.* **A 504** (2003) 331.

[25] M. Moszynski et al., *Comparative study of avalanche photodiodes with different structures in scintillation detection*, *IEEE Trans. Nucl. Sci.* **48** (2001) 1205.

[26] *Windowless large area APDs*, Advanced Photonix Inc. Application Note (1999).

[27] A.Q.R. Baron and S.L. Ruby, *Time resolved detection of X-rays using large area avalanche photodiodes*, *Nucl. Instrum. Meth.* **A 343** (1994) 517.

[28] T.W. Barnard et al, *Solid-state detector for ICP-OES*, *Anal. Chem.* **65** (1993) 1231.

[29] G.F. Knoll, *Radiation detection and measurements*, third edition, John Wiley & Sons, New York U.S.A. (2000).

[30] http://physics.nist.gov/PhysRefData/FFast/html/form.html.

[31] M. Moszynski, M. Szawlowski, M. Kapusta and M. Balcerzyk, *Large area avalanche photodiodes in scintillation and X-rays detection*, *Nucl. Instrum. Meth.* A **485** (2002) 504.

[32] F: Perotti and C. Fiorini, *Observed energy dependence of Fano factor in silicon at hard X-ray energies*, *Nucl. Instrum. Meth.* **A 423** (1999) 356.

[33] P.W. Nicholson, *Nuclear electronics*, Wiley-Interscience Publication, John Wiley & Sons, London U.K. (1974).

[34] R.J. McIntyre, *Multiplication noise in uniform avalanche diodes*, *IEEE Trans. Electron Devices* **13** (1966) 164.

[35] R.J. McIntyre, *The distribution of gains in uniformly multiplying avalanche photodiodes: theory*, *IEEE Trans. Electron Devices* **19** (1972) 703.

[36] *Noise characteristics of Advanced Photonix avalanche photodiodes*, Advanced Photonix Inc. Application Note (1991).

[37] L. Ludhova et al., *Planar LAAPDs: temperature dependence, performance, and application in low-energy X-ray spectroscopy*, *Nucl. Instrum. Meth.* **A 540** (2005) 169.

[38] M. Moszynski et al., *Performance of large-area avalanche photodiodes at liquid nitrogen temperature*, *IEEE Trans. Nucl. Sci.* **49** (2002) 971.

[39] L.M.P. Fernandes, P.C.P.S. Simões, J.M.F. dos Santos and R.E. Morgado, *Digital rise-time discrimination of large-area avalanche photodiode signals in X-ray detection*, *IEEE Trans. Nucl. Sci.* **49 (**2002) 1699.

[40] V.N. Solovov, V. Chepel, M.I. Lopes, R. Ferreira Marques and A.J.P.L. Policarpo, *Study of large area avalanche photodiodes for detecting liquid xenon scintillation*, *IEEE Trans. Nucl. Sci.* **47** (2000) 1307.

[41] V.N. Solovov, A. Hitachi, V: Chepel, M.I. Lopes, R. Ferreira Marques and A.J.P.L. Policarpo, *Detection of scintillation light of liquid xenon with a LAAPD*, *Nucl. Instrum. Meth.* **A 488** (2002) 572.

[42] T. Takahashi, S. Himi, M. Suzuki, J. Ruan and S. Kubota, *Emission spectra from Ar-Xe, Ar-Kr, Ar-N2, Ar-CH4, Ar-CO2 and Xe-N2 gas scintillation proportional counters*, *Nucl. Instrum. Meth.* **A 205** (1983) 591.

[43] C.M.B. Monteiro, L.M.P. Fernandes, J.A.M. Lopes, J.F.C.A. Veloso and J.M.F. dos Santos, *Detection of VUV photons with large-area avalanche photodiodes*, *Appl. Phys.* **B 81** (2005) 531.

[44] C.A.N. Conde and A.J.P.L. Policarpo, *A gas proportional scintillation counter*, *Nucl. Instrum. Meth.* **53** (1967) 7.

[45] A.J.P.L. Policarpo, *The gas proportional scintillation counter*, *Space Sci. Instrum.* **3** (1977) 77.

[46] J.M.F. dos Santos et al., *Development of portable gas proportional scintillation counters for X-ray spectrometry*, *X-Ray Spectrom.* **30** (2001) 373.

[47] J.M.F. dos Santos, A.C.S.S.M. Bento and C.A.N. Conde, *The dependence of the energy resolution of gas proportional scintillation counters on the scintillation region to photomultiplier distance*, *IEEE Trans. Nucl. Sci.* **39** (1992) 541.

[48] B. Zhou and M. Szawlowski, *An explanation on the APD spectral quantum efficiency in the deep UV range*, Advanced Photonix, Inc. Interoffice Memo (1999).

[49] T.H.V.T. Dias, J.M.F. dos Santos, P.J.B.M. Rachinhas, F.P. Santos, C.A.N. Conde and A.D. Stauffer, *Full-energy absorption of X-ray energies near the Xe L- and K-photoionization thresholds in xenon gas detectors: simulation and experimental results*, *J. Appl. Phys.* **82** (1997) 2742.

[50] I.K. Bronic, *W values and Fano factors for electrons in rare gases and rare gas mixtures*, *Ionizing Radiation* **24** (1998) 101.

[51] J.F.C.A. Veloso et al., *Gas proportional scintillation counters for the μp Lamb-shift experiment*, *IEEE Trans. Nucl. Sci.* **49** (2002) 899.